Talanta 85 (2011) 310–316

Contents lists available at ScienceDirect

Talanta

journal homepage: www.elsevier.com/locate/talanta

# A disposable electrochemical sensor for the determination of indole-3-acetic acid based on poly(safranine T)-reduced graphene oxide nanocomposite

Tian Gan [a,c], Chengguo Hu [a,*], Zilin Chen [b], Shengshui Hu [a,c,**]

[a] Key Laboratory of Analytical Chemistry for Biology and Medicine (Ministry of Education), College of Chemistry and Molecular Sciences, Wuhan University, Wuhan 430072, PR China
[b] Department of Pharmaceutical Analysis, College of Pharmacy, Wuhan University, Wuhan 430072, PR China
[c] State Key Laboratory of Transducer Technology, Chinese Academy of Sciences, Beijing 10080, PR China

ARTICLE INFO

*Article history:*
Received 20 January 2011
Received in revised form 21 March 2011
Accepted 25 March 2011
Available online 5 April 2011

*Keywords:*
Indole-3-acetic acid
Reduced graphene oxide
Poly(safranine T)
Electropolymerization
Electrochemical sensor

ABSTRACT

A disposable electrochemical sensor for the determination of indole-3-acetic acid (IAA) based on nanocomposites of reduced graphene oxide (rGO) and poly(safranine T) (PST) was reported. The sensor was prepared by coating a rGO film on a pre-anodized graphite electrode (AGE) through dipping–drying and electrodepositing a uniform PST layer on the rGO film. Scanning electron microscopic (SEM) and infrared spectroscopic (IR) characterizations indicated that PST–rGO formed a rough and crumpled composite film on AGE, which exhibited high sensitive response for the oxidation of IAA with 147–fold enhancement of the current signal compared with bare AGE. The voltammetric current has a good linear relationship with IAA concentration in the range $1.0 \times 10^{-7}$–$7.0 \times 10^{-6}$ M, with a low detection limit of $5.0 \times 10^{-8}$ M. This sensor has been applied to the determination of IAA in the extract samples of several plant leaves and the recoveries varied in the range of 97.71–103.43%.



## 1. Introduction

Indole-3-acetic acid (IAA, Scheme 1A), the first identified auxin in the 1930s, is released by the terminal bud of a shoot and acts as a true chemical messenger regulating some important biological processes of plants, e.g., division, elongation and differentiation of cells [1]. The determination of IAA in plant is therefore of great significance for exploring its biological roles. Up to date, a variety of techniques have been employed for the detection of IAA, including chemiluminescence [2,3], liquid chromatography [4–6], gas chromatography [7], capillary electrophoresis [8–10], spectrofluorometric method [11] and enzyme-linked immunosorbent assay [12]. These techniques are either sensitive or selective to the determination of IAA, but generally suffer from the disadvantages of complex instruments and being time-consuming.

Alternatively, the unsaturated heterocyclic moiety of IAA provides a chance for the determination of IAA by electrochemical methods with high sensitivity, rapid response, low cost and simple apparatus. However, it is difficult for the determination of IAA due to its poor electrochemical activity. Recently, a variety of sensing carbonaceous materials, such as carbon fiber [13], graphite [14,15], carbon nanotube [16,17] and boron-doped diamond [18], are employed for the determination of IAA. Unfortunately, the electrochemical detection of IAA was usually performed at a relatively positive potential with a wide peak shape in acidic media, which significantly suppress the sensitivity and selectivity of the sensors. Thus, the development of new carbonaceous-based catalysts of IAA has become important for constructing high-performance electrochemical sensors.

Graphene, emerging as a true two-dimensional material, has attracted considerable attention in both experimental and theoretical scientific communities because of its interesting physical/chemical properties (e.g., high surface area, excellent conductivity, easy production and functionalization, and good biocompatibility) [19]. The applications of graphene or graphene-based nanocomposites in electrochemical sensors with high sensitivity and selectivity are widely reported, such as $H_2O_2$ [20,21], NADH [22,23], trinitrotoluene [24,25], glucose [26], biomolecules and drugs [27,28] sensors. In addition, several works have demonstrated that graphene usually exhibits better electroanalytical [29–31] or electrochemical performance [32] than the extensively used carbon nanotubes (CNTs).

In this work, a disposable electrochemical sensor based on reduced graphene oxide (rGO) and poly(safranine T) (PST) for high-sensitive determination of IAA was reported. This IAA sensor was prepared by simple dipping–drying and electrodeposition meth-

* Corresponding author. Tel.: +86 27 87881642; fax: +86 27 68754067.
** Corresponding author at: Key Laboratory of Analytical Chemistry for Biology and Medicine (Ministry of Education), College of Chemistry and Molecular Sciences, Wuhan University, Wuhan 430072, PR China. Tel.: +86 27 87881642; fax: +86 27 68754067.
*E-mail addresses:* cghu@whu.edu.cn (C. Hu), sshu@whu.edu.cn (S. Hu).

0039-9140/$ – see front matter © 2011 Elsevier B.V. All rights reserved.
doi:10.1016/j.talanta.2011.03.070

**Table 1**
Comparison of analytical performance at different modified electrodes for the electrochemical determination of IAA.

| Sensing materials | Sensitivity (μA/μM) | Linear range (μM) | Detection limit (μM) | Peak potential (V) | Ref. |
|---|---|---|---|---|---|
| Carbon fiber | 0.0182 | 1.48–21.00 | – | 0.97 (vs. Ag/AgCl) | [13] |
| Graphite | 2.55 | 0.05–2.00 | 0.02 | 0.66 (vs. SCE) | [14] |
| Graphite–polyurethane | 0.003 ± 0.0045 | 1.3–94.7 | 0.15 | 0.88 (vs. SCE) | [15] |
| Nano Au/MWNTs/chitosant | 0.14 | 5.0–200.0 | 8.33 | 0.78 (vs. SCE) | [16] |
| MWNT | – | 0.1–50.0 | 0.02 | 0.68 (vs. SCE) | [17] |
| Boron–doped diamond | – | 5.0–50.0 | 1.22 | 0.93 (vs. Ag/AgCl) | [18] |
| PST–rGO | 9.95 | 0.1–7.0 | 0.05 | 0.49 (vs. SCE) | Our work |

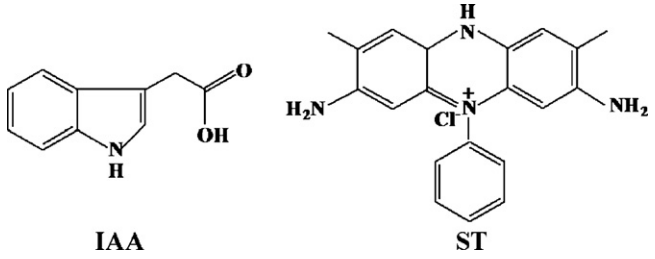


**Scheme 1.** Chemical structures of IAA and safranine T.

ods, which can produce PST–rGO composite film with surface properties similar to GO-based nanocomposites [33]. Moreover, this sensor exhibited a lower oxidation potential and a higher sensitivity for the determination of IAA compared with most of the previous works (Table 1), which was successfully employed for the determination of IAA in plant samples and testified by high performance liquid chromatography method. The present work not only proposed a simple method for the further functionalization of graphene by organic dyes, but also demonstrated that graphene may have predominant advantages over CNTs for constructing electrochemical sensors of special analytes, including easy production, facile surface modification, high-density surface active sites and excellent solvent dispersion.

## 2. Experimental

### 2.1. Chemicals and materials

Graphite powder (specpure), safranine T (ST) and N,N-dimethylformamide (DMF) (analytical reagent) were purchased from Sinopharm Group Chemical Reagent Co., Ltd, China. Multiwalled carbon nanotubes (MWNTs) (Nanotimes Co., Chengdu, China) were dispersed into 70% $HNO_3$ with sonication and refluxed at 120 °C for 14 h to eliminate impurities such as metal catalyst and amorphous products. IAA (Aldrich) was dissolved into methanol to prepare $1.0 \times 10^{-3}$ M standard stock solution, which was diluted by methanol to desired concentrations before use. $Na_2HPO_4$–$C_4H_2O_7$ buffer was prepared from 0.2 M $Na_2HPO_4$ and 0.1 M $C_4H_2O_7$ water solution, using NaOH and HCl to adjust the final pH. All other chemicals were of analytical grade and used without further purification. The water used was re-distilled.

### 2.2. Apparatus

Cyclic voltammetry (CV), differential pulse voltammetry (DPV) and linear sweep voltammetry (LSV) were carried out with a CHI 660A electrochemical analyzer (Chenhua Instruments, China). A conventional three-electrode system, consisting of a PST–rGO/GE, a saturated calomel reference electrode (SCE) and a platinum wire auxiliary electrode, was employed.

Field emission scanning electron microscopy (SEM) images were performed on Sirion 200 field scanning electron microscope (FEI, Holland). Fourier transform infrared spectroscopy (FTIR) spectra were measured with EQUINOX 55 (Bruker, Germany).

The high performance liquid chromatography-ultraviolet (HPLC-UV) analysis was conducted on an Agilent 1100 series HPLC-UV system (Agilent Technologies, USA) according to the report [4]. A C18 column (Lichrospher-ODS, 5-μm particle size, 200 mm × 4.6 mm) was used for the separation. The HPLC was performed by using methanol-buffer solution (containing 50 mM NaAc/HAc, pH = 3.5) (v/v = 40/60) with the flow rate of 1 mL $min^{-1}$ as the mobile phase. The UV wavelength was set at 254 nm.

### 2.3. Synthesis of reduced graphene oxide

Graphite oxide (GO), prepared from natural graphite flakes by a modified Hummer's method [34], was reduced by $NaBH_4$ in a steam bath to produce the reduced graphene oxide (rGO) [35]. At last, 4.0 mg rGO was dispersed in 2.0 mL water with sonication for 2 h to prepare the aqueous suspension of rGO.

### 2.4. Preparation of the IAA sensor

Graphite electrodes (GEs) were made according to our previous work from pencil leads (diameter 0.7 mm, black lead of degree HB, comprising about 19 wt% clay and 81 wt% graphite, purchased from a local market) [36]. A GE was anodized at +1.80 V for 240 s in a pH 8.0 $Na_2HPO_4$–$C_4H_2O_7$ buffer, and then scanned between 1.20 and 1.80 V until stable cyclic voltammograms were obtained. The resulting anodized GE (AGE) was rinsed with water before further use.

An AGE was firstly immersed in 2.0 mg $mL^{-1}$ rGO suspension for 30 min, taken out from the solution, dried in the air. Then potentially swept in 0.5 mM ST with the electrolyte of 100 mM $H_2SO_4$ and 100 mM $KNO_3$ from −0.90 to 1.70 V at a scan rate of 50 mV $s^{-1}$ for 20 cycles. The prepared PST–rGO film modified AGE was carefully rinsed with water and air dried, which was denoted as PST–rGO/AGE or IAA sensor. The IAA sensor can be renewed by cyclic sweeping in a pH 8.0 $Na_2HPO_4$–$C_4H_2O_7$ buffer for 20 cycles in the range of 1.20–1.80 V.

The fabrication of PST–MWNT or PST–GO film modified AGE was similar to that of PST–rGO except that the suspension of rGO was replaced by 2.0 mg $mL^{-1}$ MWNTs in DMF or 2.0 mg $mL^{-1}$ GO in water. The resulting electrodes were denoted as PST–MWNT/AGE and PST–GO/AGE, respectively.

### 2.5. Determination of IAA

Unless otherwise stated, a pH 8.0 $Na_2HPO_4$–$C_4H_2O_7$ buffer was used as the electrolyte for IAA analysis. The analytical procedure included two steps: firstly, IAA was preconcentrated onto the surface of PST–rGO/AGE at 0.00 V for 300-s stirring. Then, differential pulse voltammograms from 0.00 to 1.00 V were recorded, and the oxidation peak current at 0.49 V was measured.

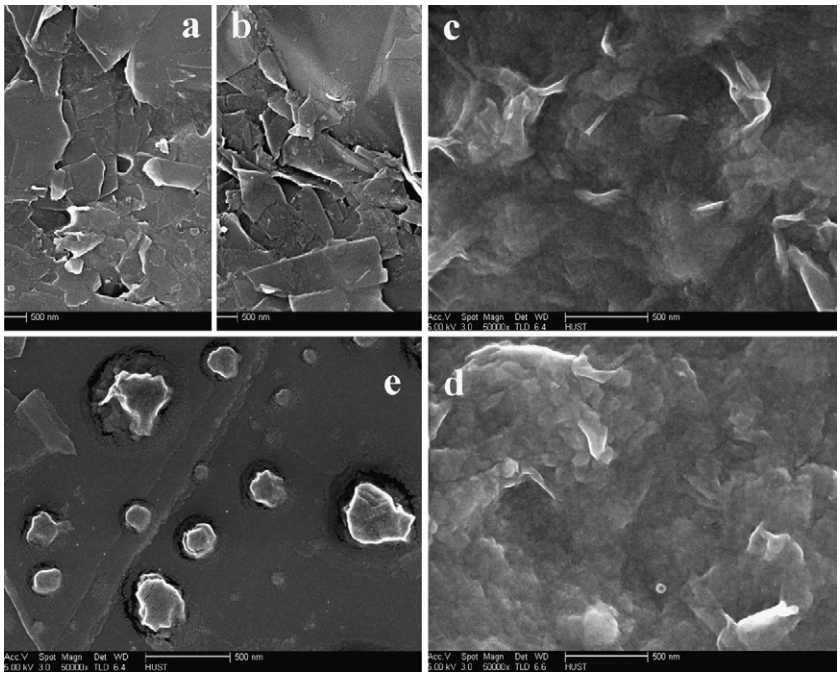


**Fig. 1.** SEM images of GE (a), AGE (b), rGO/AGE (c), PST–rGO/AGE (d) and PST/AGE (e).

## 3. Results and discussion

### 3.1. Characterizations of PST–rGO film by SEM and FTIR

The PST–rGO film on AGE was characterized by SEM (Fig. 1). It is clear that the surface of GE is completely covered by sheet-like graphite particles (a), and the anodized treatment causes slight coarsening of the electrode surface (b). By a simple immersion and drying procedure, a compact and crumpled film of rGO is formed on AGE with plenty of particle-like protuberances (c), which is similar to rGO films reported by Guo [32]. The electropolymerization of PST on rGO/AGE produces a slightly rougher surface but with similar surface morphology to rGO/AGE (d), suggesting the formation of a uniform and ultrathin PST film. In contrast, PST only forms a mirror-like smooth surface on AGE, which was decorated with some rigid large particles (e).

ST (Scheme 1B) is a water-soluble cationic dye. The oligomers and polymer chains of PST can be formed on the electrode surface through a simple and controllable electropolymerization method. Pauliukaite et al. revealed that the electrosynthetic mechanism of PST includes the formation of dications and their reaction with other monomer molecules of ST, together with deprotonation [37]. FTIR was employed to characterize the synthesis and the structure of the PST–rGO composite (Fig. 2). As shown in curve a, the spectra of rGO show only a few IR features with the peaks at 3442 $cm^{-1}$ $\nu$(O–H) and 1641 $cm^{-1}$ $\delta$(HOH) [38]. In contrast, ST (curve b) and PST–rGO (curve c) possess some characteristic IR absorptions: (i) the wide stretching vibration of N–H in ST at 3405 $cm^{-1}$ [39], which overlaps with the peak at 3442 $cm^{-1}$ of rGO and leads to a strong peak at 3440 $cm^{-1}$ on PST–rGO; (ii) the aromatic stretching vibration of C=C and the $NH_2$ scissoring of ST at 1639 $cm^{-1}$ and 1607 $cm^{-1}$ [39] overlap with the absorption of rGO at 1641 $cm^{-1}$ forming an enhanced peak at 1639 $cm^{-1}$ on PST–rGO; (iii) the peaks at 1530 and 1493 $cm^{-1}$ on curve g are caused by aromatic $\nu$(C=C), which shift to 1546 and 1514 $cm^{-1}$, respectively when the polymer of ST is synthesized [39]; (iv) the asymmetric $CH_3$ deformation of PST–rGO at 1462 $cm^{-1}$ has a slight positive shift compared to ST (1456 $cm^{-1}$) [39]. These FTIR data demonstrate the deposition of PST on rGO, which are well accord with the structure of PST [37].

### 3.2. Electrochemical behaviors of IAA

The electrochemical behaviors of $1.0 \times 10^{-4}$ M IAA at PST–rGO/AGE were investigated by CV (Fig. 3). Clearly, two oxidation peaks ($I_a$ and $II_a$) appear in first cycle with the peak potentials ($E_p$) at 0.56 V and 0.64 V, respectively. A weak reduction peak ($III_c$) located at −0.05 V appears in the reverse sweep (Fig. 3A). In the second cycle, a new weak oxidation peak ($III_a$) at 0.26 V is observed, which forms a redox couple with peak $III_c$. As no redox peaks were observed for PST–rGO/AGE in the blank buffer (not shown), the redox peaks in Fig. 3A should arise from the electrochemical reactions of IAA or its products. Interestingly, when the potential sweep starts at 0.55 V, a potential giving no chance for the peak $I_a$ to oxidize completely, peak $II_a$ completely

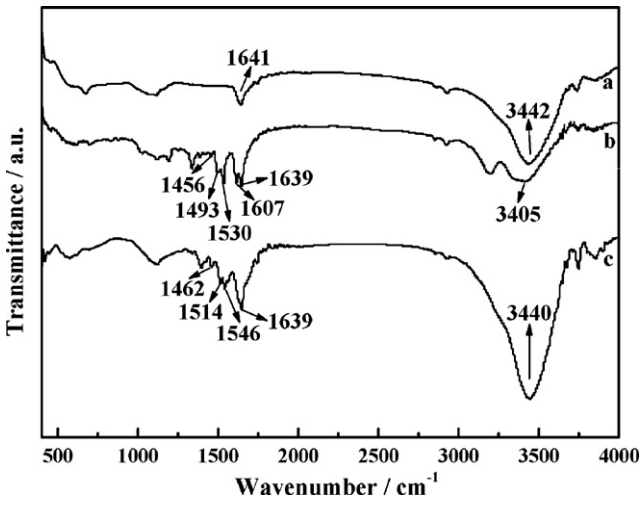


**Fig. 2.** IR spectra of rGO (a), ST (b) and PST–rGO hybrid (c).

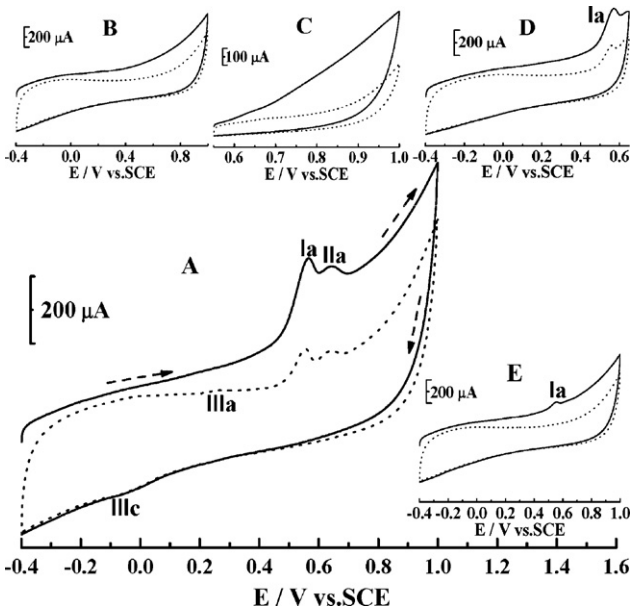


**Fig. 3.** Loopy cyclic voltammograms of PST–rGO/AGE under different conditions: (A). in $1.0 \times 10^{-4}$ M IAA from −0.40 to 1.00 V; (B) in blank buffer from −0.40 to 1.00 V; (C) in $1.0 \times 10^{-4}$ M IAA from 0.55 to 1.00 V; (D) in $1.0 \times 10^{-4}$ M IAA from −0.40 to 0.65 V; (D) in $5.0 \times 10^{-6}$ M IAA from −0.40 to 1.00 V. Scan rate: 100 mV $s^{-1}$. The solid and the dash lines stand for the first and the second cycles, respectively.

disappears (Fig. 3B). This result suggests that peak $II_a$ is related to the oxidation of the product of peak $I_a$. If the potential sweep is confined in the range of −0.4–0.65 V, the redox peaks $III_c$ and $III_a$ disappear (Fig. 3C), indicating that this redox couple may also result from the product of peak $II_a$. The voltammograms of IAA at low concentrations are much different (Fig. 3D), i.e., the peak $II_a$ and the redox couple $III_c/III_a$ for $5.0 \times 10^{-6}$ M IAA disappear, which are well consistent with previous reports [17,40].

### 3.3. Enhanced responses of IAA at PST–rGO/AGE

In order to obtain most sensitive electrochemical response and best peak shape for IAA, DPV technique was used. Fig. 4 shows the DPV responses of IAA at different graphite electrodes.

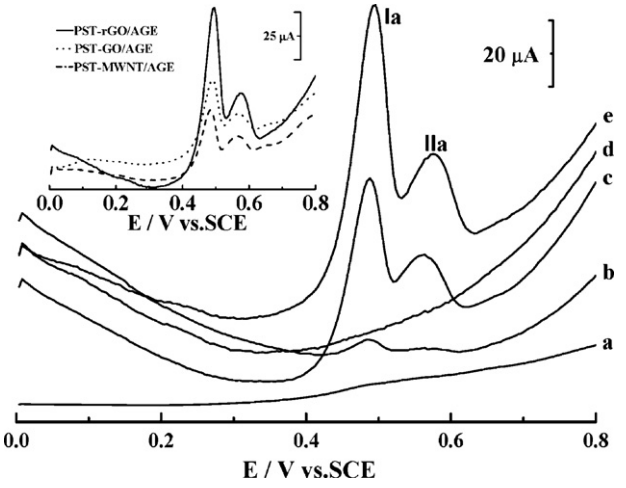


**Fig. 4.** DPV responses of $7.0 \times 10^{-6}$ M IAA at GE (a), AGE (b), rGO/AGE (c) and PST–rGO/AGE (e). Curve d responds to the DPV behavior of PST–rGO/AGE in blank buffer. Inset: the comparison of DPV behaviors of $7.0 \times 10^{-6}$ M IAA at PST–rGO/AGE, PST–GO/AGE and PST–MWNT/AGE Accumulation time: 300 s, amplitude: 50 mV, pulse width: 50 ms, pulse period: 200 ms..

In a $Na_2HPO_4$–$C_4H_2O_7$ buffer (pH 8.0), $7.0 \times 10^{-6}$ M IAA yields an almost indiscernible oxidation peak (i.e., peak $I_a$) at 0.50 V with a peak current $I_p$ of 0.46 μA at GE for 300 s accumulation (curve a). The oxidation peak becomes noticeable at AGE ($I_p$ = 3.91 μA, curve b), probably due to the enlarged surface area and the introduction of active sites by anodization. The oxidation current peak $I_a$ significantly increases ($I_p$ = 39.49 μA) and peak $II_a$ begins to appear when a rough and compact rGO film is formed on AGE (curve c), which are further enhanced ($I_{pa}$ = 67.56 μA) when an additional PST film is electrochemically deposited (curve d). Moreover, the oxidation potential of IAA on rGO/AGE hardly changes in comparison with that on GE, suggesting the same graphitic nature of rGO and graphite. As peak $I_a$ is more sensitive than peak $II_a$, peak $I_a$ can be selected for the electrochemical detection of IAA.

The DPV responses of IAA at PST–GO and PST–MWNT composites are also examined (inset of Fig. 4). Clearly, both GO and MWNT apparently enlarge the electrochemical signal of IAA, but their sensitizing effects are not as good as rGO. The better performance of rGO compared with GO is probably attributed to the stronger accumulation of aqueous-insoluble IAA on more hydrophobic rGO [41]. In the case of MWNT, the interesting promotional performance of rGO may be correlated with its highly conductivity, metallic conductance and enhanced size effect [30]. Besides these, the unique two-dimensional structure of rGO is more favorable for the good adsorption of both ST and IAA on its six-carbon rings via $\pi$–$\pi$ interaction than one-dimensional MWNT. Moreover, the large scale production of GO or rGO can be easily achieved in labs all over the world without the use of special instruments or reagents. Based on these results, it is clear that rGO or GO is an excellent sensing material for electrochemical sensors, which can form uniform and compact carbonaceous nanostructures on the electrode surface with high chemical stability, high surface area and high-density electroactive sites.

### 3.4. Optimization of detection conditions

#### 3.4.1. Influence of solution pH

Influence of solution acidity on the oxidation behavior of $1.0 \times 10^{-5}$ M IAA at PST–rGO/AGE in $Na_2HPO_4$–$C_4H_2O_7$ buffers in the range of pH 2.4–10.0 was tested. The results indicated that the oxidation current reached the highest at pH 8.0 and kept almost unchanged at higher pH value. According to the report [14], IAA ($pK_a$ = 4.75) exists in anionic form when pH is higher than 4.75, so the positive-charged PST film with plenty amido can strongly attract IAA according to the principle of electrostatic interaction and therefore lead to the enhanced electrochemical response of IAA in alkalescent environment. Meanwhile, the oxidation peak potential showed a good linear relationship with the solution pH (i.e., $E_p/V = -0.036$ pH +0.839, $R$ = 0.996), implying that the ratio of electron-to-proton involved in the oxidation reaction of peak $I_a$ was 2/1. A solution of $Na_2HPO_4$–$C_4H_2O_7$ buffer with pH 8.0 was therefore selected as the optimal electrolyte for the detection of IAA in the following experiments.

#### 3.4.2. Influence of electropolymerization conditions

The optimal electrolytes for electropolymerizing PST film on rGO/AGE were tested, including a mixture of 100 mM $H_2SO_4$ and 100 mM $KNO_3$, 50 mM phosphate buffer (pH 5.5) and 100 mM $KNO_3$, 50 mM phosphate buffer (pH 7.0) and 100 mM $KNO_3$, 100 mM $H_2SO_4$ and 100 mM KCl. The results suggested that PST–rGO/AGE prepared in 100 mM $H_2SO_4$ + 100 mM $KNO_3$ possessed the most sensitive electrochemical signal of IAA, which well accorded with a previous report, i.e., ST could form a stable polymer in acidic media and $NO_3^-$ catalysed the polymerization of ST [37].

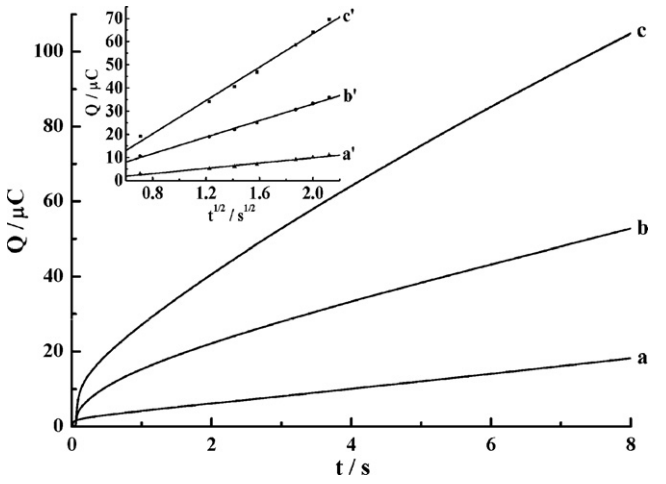


**Fig. 5.** Chronocoulometry of $1.0 \times 10^{-5}$ M IAA at GE (a), rGO/AGE (b) and PST–rGO/AGE (c). Insets show the linear relationships between charge ($Q$) and the square root of time ($t^{1/2}$) for the oxidation reactions (background subtracted) at GE (a′), rGO/AGE (b′) and PST–rGO/AGE (c′). Initial potential: 0.516 V, final potential: 0.616 V, and pulse width: 8 s.

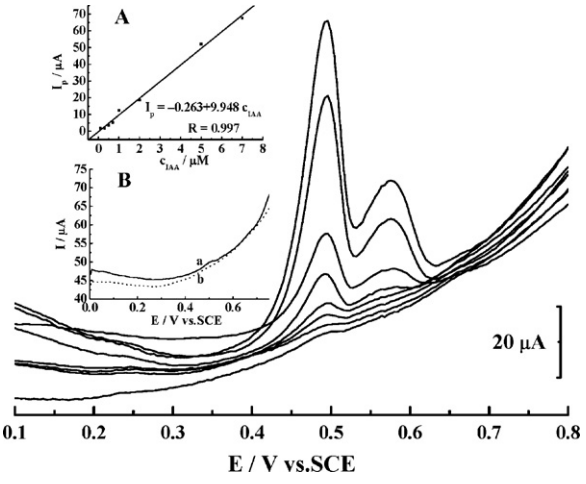


**Fig. 6.** DPV responses for IAA of various concentrations at PST–rGO/AGE (from inner to outer): $1.0 \times 10^{-7}$, $3.0 \times 10^{-7}$, $5.0 \times 10^{-7}$, $7.0 \times 10^{-7}$, $1.0 \times 10^{-6}$, $2.0 \times 10^{-6}$, $5.0 \times 10^{-6}$ and $7.0 \times 10^{-6}$ M. Inset A: the calibration graph. Inset B: the voltammograms of PST–rGO/AGE in $5.0 \times 10^{-8}$ M IAA (a) and a blank buffer (b). Other conditions are as Fig. 4.

The influences of electropolymeric potential range and electropolymeric cycles on the peak current of IAA were examined. In the first case, the initial potential changed from −0.7 to −1.0 V and the final potential was tested from 1.6 to 1.9 V. The results revealed that the highest response of IAA on PST–rGO/AGE was obtained in the potential range of −0.9–1.7 V because the redox of ST can be finished in this range. In the second case, the cycle number from 10 to 40 was tested and the highest oxidation current of IAA was achieved for 20 cycles. Fewer cycles with thinner PST film has not enough catalytic ability for IAA oxidation but more cycles may result to a too thick PST film which can embarrass the electron transfer between IAA and the electrode. Therefore, the electropolymerization of ST on rGO/AGE was performed in the range of −0.9–1.7 V for 20 cycles.

### 3.4.3. Influence of accumulation potential and time

The accumulation potential has little influence on the electrochemical responses of IAA. In this work, 0.00 V was selected by reason of convenience. The dependence of the oxidation peak current of IAA on accumulation time was also tested at this sensor. The oxidation peak current of $1.0 \times 10^{-5}$ M MeJA increases quickly from 0 to 240 s and slowly from 240 s to 300 s. At an accumulated time of 300 s, the peak current of IAA achieves the zenith. The calibration curve gradually tends to a plateau when further increases the accumulation time, indicating that the adsorption of IAA on this sensor is saturated. As a result, the accumulation time was selected as 300 s for the experiment.

### 3.5. Influence of scan rate

The influence of scan rate on the oxidation current of IAA on PST–rGO/AGE was examined in the range of 25–300 mV $s^{-1}$. The results showed that the oxidation peak current of IAA linearly increased with scan rate, indicating a diffusion-controlled electrode process. Meanwhile, the oxidation peak potential ($E_p$) positively shifted with scan rate ($\nu$), and the relationship between $E_p$ (V) and $\nu$ (mV $s^{-1}$) is in accordance with the following equation [42]:

$$E_p = E^{0'} + \frac{RT}{\alpha nF} \ln \frac{RTk^0}{\alpha nF} + \frac{RT}{\alpha nF} \ln \nu \quad (1)$$

where $k^0$ is the standard rate constant of the surface reaction, $E^{0'}$ is the formal potential, $\alpha$ is transfer coefficient of the oxidation of IAA, and other symbols have their usual meanings. According to Eq. (1), the plot of $E_p$ vs. ln $\nu$ has a good linear relationship, from which $\alpha n$ can be determined from the slop (i.e., 0.027). Assuming $\alpha = 0.5$, two electrons are involved in the oxidation of IAA. This, coupled with the above deduced electron-to-proton ratio, suggested that one proton may take part in the oxidation process. Obviously, the oxidation process of peak $I_a$ was probably a two-electron and one-proton irreversible oxidation reaction. This mechanism was well consistent with previous reports [17,43].

### 3.6. Chronocoulometry

Chronocoulometry was used to characterize the oxidation of $1.0 \times 10^{-5}$ M IAA at GE (a), rGO/AGE (b) and PST–rGO/AGE (c) (Fig. 5). After the subtraction of the background charge, the plot of charges ($Q$) against $t^{1/2}$ has a linear relationship for the oxidation reaction for GE (a′), rGO/AGE (b′) and PST–rGO/AGE (c′). According to the Cottrell equation, the diffusion coefficient of IAA ($D$) can be estimated from the intercept and slope of this plot:

$$Q = Q_{ads} + 2nFAcD^{1/2}\pi^{-1/2}t^{1/2} \quad (2)$$

where $A$ is the surface area of the working electrode, $c$ is the concentration of IAA, $Q_{ads}$ is the adsorption charge, and other symbols have their usual significances. Here, $A = 0.224$ $cm^2$, $c = 1.0 \times 10^{-5}$ M

**Table 2**
Influences of some compounds on the determination of $1.0 \times 10^{-6}$ M IAA.

| Interferents | Concentration (M) | Signal change (%) |
|---|---|---|
| Sucrose | $5.0 \times 10^{-4}$ | −0.53 |
| Glucose | $5.0 \times 10^{-4}$ | −1.97 |
| $SO_4^{2-}$ | $5.0 \times 10^{-4}$ | −3.20 |
| $PO_4^{3-}$ | $5.0 \times 10^{-4}$ | 2.13 |
| Oleic acid | $2.0 \times 10^{-4}$ | 2.02 |
| Ricinoleic acid | $2.0 \times 10^{-4}$ | 3.41 |
| $Fe^{3+}$ | $3.0 \times 10^{-5}$ | 3.46 |
| $Mg^{2+}$ | $2.0 \times 10^{-5}$ | −2.58 |
| $Cu^{2+}$ | $2.0 \times 10^{-5}$ | 3.25 |
| Soluble starch | $1.0 \times 10^{-5}$ | −5.40 |
| $CO_3^{2-}$ | $1.0 \times 10^{-5}$ | 2.94 |
| $Br^-$ | $1.0 \times 10^{-5}$ | −4.62 |
| $Fe^{2+}$ | $1.0 \times 10^{-5}$ | −3.27 |
| Gibberellic acid | $1.0 \times 10^{-5}$ | 4.36 |
| Abscisic acid | $1.0 \times 10^{-5}$ | −3.26 |
| Salicylic acid | $5.0 \times 10^{-6}$ | 4.74 |
| Methyl dihydrojasmonate | $1.0 \times 10^{-6}$ | −6.24 |
| Jasmone | $1.0 \times 10^{-6}$ | −6.17 |
| Methyl jasmonate | $1.0 \times 10^{-6}$ | −6.95 |

**Table 3**
Determination results of IAA in plant leaves.

| Samples | This sensor ($n=6$) | | | HPLC ($n=6$) | | |
|---|---|---|---|---|---|---|
| | Concentration (μM) | Recovery (%) | RSD (%) | Concentration (μM) (n = 6) | Recovery (%) | RSD (%) |
| *Cinnamomum camphora* | 2.79 | 98.41 | 2.26 | 3.08 | 105.34 | 1.06 |
| *Prunus yedoensis Mats.* | 4.74 | 101.36 | 3.11 | 4.56 | 99.47 | 3.42 |
| *Firmiana simplex* | 2.08 | 100.48 | 2.93 | 1.87 | 102.64 | 2.85 |

and $n=2$, so the deduced values of $D$ are 0.00014, 0.0013 and 0.0054 $cm^2\ s^{-1}$ for GE, rGO/AGE and PST–rGO/AGE, respectively. In addition, $Q_{ads}$ can be obtained by differentiating the intercepts of the plots of $Q$ versus $t^{1/2}$ in the presence and the absence of IAA. According the equation $Q_{ads} = nFA\Gamma$, the values of the surface concentration ($\Gamma$) of IAA at the three electrodes are 0.035, 0.061 and 0.20 nmol $cm^{-2}$ for GE, rGO/AGE and PST–rGO/AGE, respectively, which further identify a strong adsorption capacity of the PST–rGO film.

### 3.7. Analytical application

The calibration curve of IAA at PST–rGO/AGE was characterized by DPV (Fig. 6). The linear relationship between the concentration of IAA (c/μM) and the oxidation peak current ($I_p$/μA) can be described as $I_p = -0.263 + 9.948$ c ($R = 0.997$) in the range of $1.0 \times 10^{-7}$–$7.0 \times 10^{-6}$ M, along with a detection limit of $5.0 \times 10^{-8}$ M for 300 s accumulation at 0.0 V. The relative standard deviations (RSD) are 2.34% and 6.86% for ten parallel detections of $2.0 \times 10^{-6}$ M IAA on the same and different PST–rGO/AGEs, respectively, suggesting the good reproducibility of this IAA sensor.

### 3.8. Interferences

The interferences from some potential compounds on the determination of IAA at this sensor were evaluated. The results (Table 2) showed that no interference can be observed for 500-fold of sucrose, glucose, $SO_4^{2-}$, $PO_4^{3-}$; 200-fold of oleic acid and ricinoleic acid; 30-fold of $Fe^{3+}$; 20-fold of $Mg^{2+}$, $Cu^{2+}$; 10-fold of soluble Starch, $CO_3^{2-}$, $Br^-$, $Fe^{2+}$ in determination of $1.0 \times 10^{-6}$ M of IAA. The interferences from several phytohormones including 10-fold gibberellic acid and abscisic acid, and 5-fold salicylic acid were also negligible. However, several jasmonic acid-based auxins (e.g., methyl dihydrojasmonate, methyl jasmonate and jasmone) have slight interferences on the determination of IAA, probably due to the block of electroactive sites on PST–rGO/AGE by these oil-soluble species.

### 3.9. Detection of IAA in plant leaves

To evaluate the applicability of the proposed sensor, leaf samples from *Cinnamomum camphora*, *Prunus yedoensis Mats.* And *Firmiana simplex* were collected for the determination of IAA. The procedure for the sample treatment was as follows: 40 g leaves of each plant was treated with liquid nitrogen and then pulverized; the compounds were extracted with 80% frigorific methanol and separated by an extraction method [13]. The DPV responses of IAA in the leaves of *P. yedoensis Mats.* Are illustrated in Fig. 7. From curves a and b, it is clear that the oxidation peak current at 0.49 V ($O_2$) increases correspondingly by the addition of a standard solution of IAA, but the oxidation peak of $O_1$ at 0.32 V almost keeps unchanged. These results suggest the attribution of peak $O_2$ to IAA. Additional samples were also measured by similar procedures and the results were compared with that from HPLC, which are shown in Table 3. The results obtained by HPLC and IAA sensor are very close, confirming the applicability of the proposed sensor for the determination of IAA in real samples.

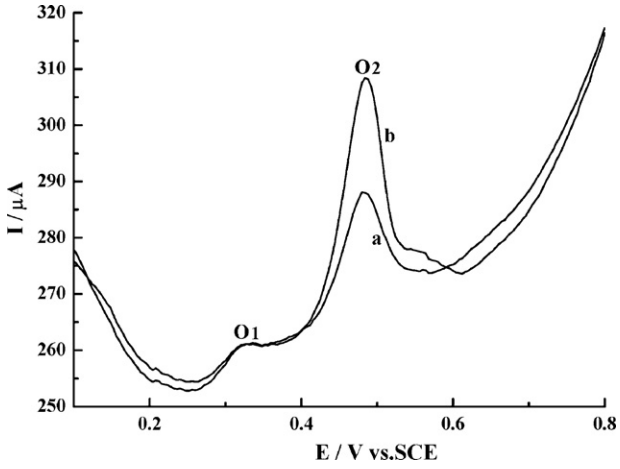


**Fig. 7.** Illustration for the determination of IAA in the leaves of *Prunus yedoensis Mats.* By a standard addition method. A: DPV of IAA in the leaf extract; b: a+$2.4 \times 10^{-6}$ M IAA standard solution. Other conditions are as Fig. 4.

## 4. Conclusion

A disposable and sensitive electrochemical sensor of IAA based on rGO composites was reported. This IAA sensor was fabricated by a simple dipping–drying and electrodeposition method. The sensing layer possessed a compact and crumpled rGO nanostructured surface with high surface area and excellent electrochemical activity. Electrochemical characterizations revealed that the response of IAA at this sensor was enhanced for 147 fold compared with the bare electrode, and rGO also exhibited better performance than widely used GO or CNTs. This sensor has the merits of a wide calibration range and a low detection limit, which has been applied to the detection of IAA in extract samples of several plant leaves.

## Acknowledgements

This research is supported by the National Nature Science Foundation of China (Nos. 90817103, 20805035 and 31070885).

## References

[1] E.A. Schneider, F. Wightman, Annu. Rev. Plant Physiol. 25 (1974) 487–513.
[2] S.Q. Han, Microchim. Acta 168 (2010) 169–175.
[3] T. Kamidate, H. Andou, Chem. Lett. 7 (1999) 557–558.
[4] Y.L. Wu, B. Hu, J. Chromatogr. A 1216 (2009) 7657–7663.
[5] J.H. Fu, J.F. Chu, J.D. Wang, C.Y. Yan, Chin. J. Anal. Chem. 37 (2009) 1324–1327.
[6] Z.J. Xi, Z.J. Zhang, Y.H. Sun, Z.L. Shi, W. Tian, Talanta 79 (2009) 216–221.
[7] C. LaMotte, X.Y. Li, W. Jacobs, E. Epstein, Plant Growth Regul. 36 (2002) 19–25.
[8] N.A. Assuncao, S.C.C. Arruda, A.P. Martinelli, E. Carrilho, J. Braz. Chem. Soc. 20 (2009) 183–187.
[9] X.B. Yin, D.Y. Liu, J. Chromatogr. A 1212 (2008) 130–136.
[10] T.F. Jiang, Z.H. Lv, Y.H. Wang, M.E. Yue, Anal. Sci. 22 (2006) 811–814.
[11] Y.N. Li, H.L. Wu, S.H. Zhu, J.F. Nie, Y.J. Yu, X.M. Wang, R.Q. Yu, Anal. Sci. 25 (2009) 83–88.
[12] M.A. Gussakovskaya, A.N. Blintsov, Biochemistry (Mosc.) 72 (2007) 339–344.
[13] L. Hernández, P. Hernández, F. Patón, Anal. Chim. Acta 327 (1996) 117–123.
[14] S.H. Zhang, K.B. Wu, Bull. Korean Chem. Soc. 25 (2004) 1321–1325.

[15] R.A. de Toledo, C.M.P. Vaz, Microchem. J. 86 (2007) 161–165.
[16] X.Y. Zhang, X.M. Liu, W.L. Liu, M. Yang, Z.Q. Zhang, Chem. J. Chin. Univ. Chin. 31 (2010) 33–37.
[17] K.B. Wu, Y.Y. Sun, S.S. Hu, Sens. Actuators B: Chem. 96 (2003) 658–662.
[18] Y. Yardim, M.E. Erez, Electroanalysis 23 (2011) 667–673.
[19] H.Q. Chen, M.B. Müller, K.J. Gilmore, G.G. Wallace, D. Li, Adv. Mater. 20 (2008) 3557–3561.
[20] W. Lv, M. Guo, M.H. Liang, F.M. Jin, L. Cui, L.J. Zhi, Q.H. Yang, J. Mater. Chem. 20 (2010) 6668–6673.
[21] Q. Zhang, Y. Qiao, F. Hao, L. Zhang, S.Y. Wu, Y. Li, J.H. Li, X.M. Song, Chem. Eur. J. 16 (2010) 8133–8139.
[22] C.S. Shan, H.F. Yang, D.X. Han, Q.X. Zhang, A. Ivaska, L. Niu, Biosens. Bioelectron. 25 (2010) 1504–1508.
[23] W.J. Lin, C.S. Liao, J.H. Jhang, Y.C. Tsai, Electrochem. Commun. 11 (2009) 2153–2156.
[24] L.H. Tang, H.B. Feng, J.S. Cheng, J.H. Li, Chem. Commun. 46 (2010) 5882–5884.
[25] S.J. Guo, D. Wen, Y.M. Zhai, S.J. Dong, E.K. Wang, ACS Nano 4 (2010) 3959–3968.
[26] S. Alwarappan, C. Liu, A. Kumar, C.Z. Li, J. Phys. Chem. C 114 (2010) 12920–12924.
[27] Y.R. Kim, S. Bong, Y.J. Kang, Y. Yang, R.K. Mahajan, J.S. Kim, H. Kim, Biosens. Bioelectron. 25 (2010) 2366–2369.
[28] Y.J. Guo, S.J. Guo, J.T. Ren, Y.M. Zhai, S.J. Dong, E.K. Wang, ACS Nano 4 (2010) 4001–4010.
[29] L. Tan, K.G. Zhou, Y.H. Zhang, H.X. Wang, X.D. Wang, Y.F. Guo, H.L. Zhang, Electrochem. Commun. 12 (2010) 557–560.
[30] Y. Wang, Y.M. Li, L.H. Tang, J. Lu, J.H. Li, Electrochem. Commun. 11 (2009) 889–892.
[31] S.R.C. Vivekchand, C.S. Rout, K.S. Subrahmanyam, A. Govindaraj, C.N.R. Rao, J. Chem. Sci. 120 (2008) 9–13.
[32] C.X. Guo, H.B. Yang, Z.M. Sheng, Z.S. Lu, Q.L. Song, C.M. Li, Angew. Chem. Int. Ed. 49 (2010) 3014–3017.
[33] T. Cassagneau, F. Guérin, J.H. Fendler, Langmuir 16 (2000) 7318–7324.
[34] T.S. Sreeprasad, A.K. Samal, T. Pradeep, J. Phys. Chem. C 113 (2009) 1727–1737.
[35] A.B. Bourlinos, D. Gournis, D. Petridis, T. Szabó, A. Szeri, I. Dékány, Langmuir 19 (2003) 6050–6055.
[36] G.G. Hao, D.Y. Zheng, T. Gan, C.G. Hu, S.S. Hu, J. Exp. Nanosci. 6 (2011) 13–28.
[37] R. Pauliukaite, A. Selskiene, A. Malinauskas, C.M.A. Brett, Thin Solid Films 517 (2009) 5435–5441.
[38] M. Herrera-Alonso, A.A. Abdala, M.J. McAllister, I.A. Aksay, R.K. Prud'homme, Langmuir 23 (2007) 10644–10649.
[39] G. Ćirić-Marjanović, N.V. Blinova, M. Trchová, J. Stejskal, J. Phys. Chem. B 111 (2007) 2188–2199.
[40] T. Hu, G. Dryhurst, J. Electroanal. Chem. 362 (1993) 237–248.
[41] S. Stankovich, D.A. Dikin, R.D. Piner, K.A. Kohlhaas, A. Kleinhammes, Y.Y. Jia, Y. Wu, S.T. Nguyen, R.S. Ruoff, Carbon 45 (2007) 1558–1565.
[42] E. Laviron, Electroanal. Chem. Inter. Electrochem. 52 (1974) 355–393.
[43] T. Hu, G. Dryhurst, J. Electroanal. Chem. 432 (1997) 7–18.